CFD Modeling and Simulation in Materials Processing 2016
Edited by: Laurentiu Nastac, Lifeng Zhang, Brian G. Thomas, Miaoyong Zhu, Andreas Ludwig, Adrian S. Sabau, Koulis Pericleous, and Hervé Combeau
TMS (The Minerals, Metals & Materials Society), 2016

LARGE EDDY SIMULATIONS OF THE EFFECTS OF DOUBLE-RULER ELECTROMAGNETIC BRAKING AND NOZZLE SUBMERGENCE DEPTH ON MOLTEN STEEL FLOW IN A COMMERCIAL CONTINUOUS CASTING MOLD

Kai Jin[1], Surya P. Vanka[1], Brian G. Thomas[1], Xiaoming Ruan[2]

[1]Department of Mechanical Science and Engineering;
1206 W Green St.; Urbana, IL 61801, USA.
[2]Steelmaking Research Department, Research Institute Baoshan Iron &Steel Co., Ltd.;
889 Fujin Rd., Shanghai 201900, P. R. China.

Keywords: Continuous casting, Electromagnetic braking, Large eddy simulation

Abstract

In steel continuous casting, flow in the mold region is related to many quality problems such as surface defects and slag entrainment. An electromagnetic braking (EMBr) system is a method to control the steel flow field to minimize defects and capture inclusions. The position of the port of the Submerged Entry Nozzle (SEN) and the peak magnetic field both affect the performance of the EMBr. In the present work, an efficient multi-GPU based code, CUFLOW, is used to perform Large Eddy Simulations of the turbulent flow by solving the time-dependent Navier-Stokes equations in a domain that includes the slide gate, SEN and mold region. The computations were first validated by comparing the predicted surface velocity with plant measurements. Subsequently, eight LES simulations were conducted to study the effects of different EMBr values and SEN depths. The flow patterns in various regions are presented. The results show that applying EMBr greatly lowers top surface velocities and turbulent fluctuations.

Introduction

In the continuous casting process for making steel, electromagnetic devices are often used to modify the flow pattern in the mold region. The magnetic field can be either static (applying a DC current to electromagnets) or dynamic in which an AC current is applied. The static magnetic field in turn generates a Lorentz force field that acts against the flow. This type of configuration is therefore referred to as an electromagnetic braking (EMBr) system. Based on the DC electromagnet's shape and location, there are usually three types of magnetic field configurations [1]: local, single ruler and double-ruler [2–7]. The differences between these configurations are discussed elsewhere [1]. This work focuses on the double-ruler configuration that is widely used in industry and commonly known as Flow Control Mold (FC-Mold). In the FC-Mold, two rectangular magnets are placed across the entire mold width, with one positioned near the meniscus and the other below the nozzle port [1–7].

Owing to the hostile environment of the extremely hot molten steel, it is difficult to conduct experiments in real casters. Computational models are widely used [2–9] as tools to understand the physics of the process, and improve and optimize the operation. A large number of the previous numerical studies solved the Reynolds Averaged Navier Stokes (RANS) equations with attention paid to the time mean flow behavior in the mold [2,3,7]. Recent developments in parallel computing technology have enabled high-fidelity Large Eddy Simulations (LES) to become feasible and have been recently performed by a few researchers to study the transient aspects of the turbulent fluid flow [4–6,9].

The FC-Mold EMBr arrangement followed in industry can affect both the mean flow behavior and the transient flow structure in the mold [5–7]. It also reduces the mean surface velocity and fluctuations normal to the free surface [2,3,5–7]. However, electromagnetic forces can also have an opposite effect on the overall flow if not used properly along with other parameters (e.g. submergence depth) [1]. With the same EMBr settings, different submergence depths may considerably change the effectiveness of local EMBr system [1]. However, to our knowledge not much attention has been paid to the effect of submergence depth and EMBr field distribution, especially for the widely used double-ruler magnetic field arrangement.

The effect of EMBr on the flow in mold has been previously studied, but the effects on the flow in the Submerged Entry Nozzle (SEN) have not been reported. Much of the work has been focused on the effects of an EMBr on the flow in the mold region without including the full SEN [2–5,8]. While some researchers have included the SEN in the computational domain, they have ignored the magnetic field above the steel-slag interface [6]. However, simulations with RANS have shown that a strong magnetic field modifies the mean flow inside the SEN and reduces its turbulent kinetic energy [7]. Therefore, high accuracy transient simulations must be conducted with inclusion of also the effects of the magnetic field on the nozzle flow.

The work presented here investigates the effect of submergence depth and EMBr on the turbulent flow in both SEN and mold regions of a real continuous caster of steel using LES. This paper first introduces the governing equations, then describes the computational models and numerical details. The model is then validated by comparing the predictions with plant measurements. The effect of submergence depth and EMBr on the flow field in the SEN, port, mold region and top surface are subsequently investigated. Finally, the important results are summarized.

Plant Measurements

Plant measurements of the magnetic fields and molten steel flow were conducted on the No. 4 caster at Baosteel, Shanghai in 2012. Top surface velocities of this conventional (230×1200 mm) continuous steel slab caster were measured with a device similar to Sub-meniscus Velocity Control (SVC) equipment. In the measurement, one end of a rod is connected to a pivot and the other end is dipped into the molten steel as shown in Figure 1. The molten steel flow impinges on the rod and induces a drag force that balances the weight of the rod and makes the rod rotate around the pivot by an angle θ. The angle is then converted into velocity of the molten steel. The SVC-like device probe was placed at quarter mold region parallel to the Wide Face (WF) of the mold and the measured steel surface velocity was recorded every 5 seconds in a 70-second time interval. The casting conditions and process parameters are given in Table I. Flow rate of the molten steel through the SEN into the mold was controlled by a slide-gate that moved between the geometric center and the Inside Radius (IR) side of the caster. For the experiments casting 1200mm wide slabs at 1.3m/min, the slide gate was 70% open, as shown in Figure 2. No argon gas was injected, and the EMBr system was also turned off during the experiment. The measured magnetic field strengths down the mold are shown in Figure 3.

Table I. Casting Parameters and Properties of the Steel

Process parameter	Value
Mold thickness (L_t)	230 mm
Mold width (L_w)	1200 mm*; 1300 mm
Slide gate opening area fraction	70%*; 80%
Submergence depth (d_{sub})	170 mm or 200 mm
SEN port downward angle	15°
Casting speed (V_c)	1.3 m/min*; 1.8 m/min
Steel density (ρ)	7000 kg/m^3
Steel dynamic viscosity (μ)	0.0063 kg/(m·s)
Steel electrical conductivity (σ)	liquid steel 714000 S/m; solid steel 787000 S/m

* Casting conditions when plant measurements were done

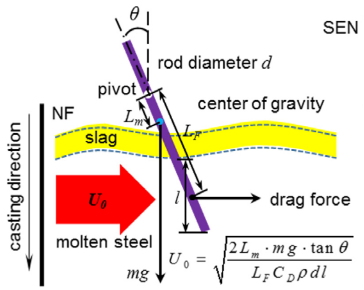

Figure 1. Schematic of SVC-like device

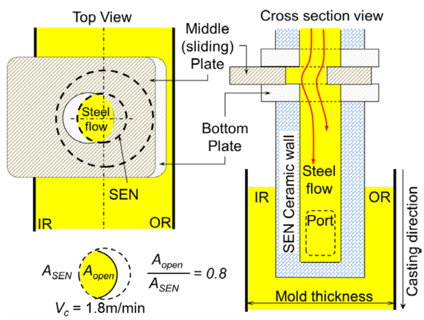

Figure 2. Slide gate position

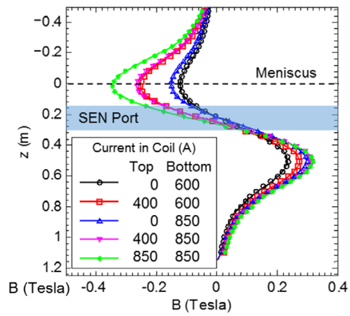

Figure 3. Magnetic fields

Governing Equations and Computational Model

A three-dimensional finite-volume computational model was applied to study the flow behavior in the caster. The governing equations and details of the model are discussed in this section.

Governing Equations for Fluid Flow

In LES, the dimensional filtered time dependent Navier Stokes equations given below are solved.

$$\nabla \cdot (\rho \mathbf{u}) = \dot{s} \tag{1}$$

$$\frac{\partial \mathbf{u}}{\partial t} + \mathbf{u} \cdot \nabla \mathbf{u} = -\frac{\nabla p}{\rho} + \nabla \cdot \left[(\nu + \nu_{sgs}) (\nabla \mathbf{u} + \nabla \mathbf{u}^T) \right] + \frac{\mathbf{F}_L}{\rho} \tag{2}$$

Here $\dot{s}$ is the sink term due to the solidifying shell, ρ is the molten steel density, $\mathbf{u}$ is filtered velocity, p is modified static pressure which includes the filtered normal stresses, $\mathbf{F}_L$ is the effect of the Lorentz force, ν is the kinematic viscosity of the molten steel and ν_{sgs} is the eddy viscosity that was computed from the coherent-structure Smagorinsky model (CSM) [10] also used in previous studies of fluid flow in steel casters with EMBr [6].

$$\nu_{sgs} = (C_s \Delta)^2 \sqrt{2 \|\mathbf{S}\|^2} \tag{3}$$

$$C_s^2 = C_{CSM}\left|\frac{Q}{E}\right|^{3/2}\left(1-\frac{Q}{E}\right) \quad \text{where} \quad Q=\frac{1}{2}\left(\|\mathbf{W}\|^2-\|\mathbf{S}\|^2\right) \quad \text{and} \quad E=\frac{1}{2}\left(\|\mathbf{W}\|^2+\|\mathbf{S}\|^2\right) \tag{4}$$

where Δ is the filter width, **S** is the filtered rate-of-strain tensor, C_{csm}=1/22 is a model constant and **W** is the filtered vorticity tensor (also known as rate of rotation tensor). The CSM model incorporates the effect of anisotropy induced by the applied magnetic fields on the filtered scales [10]. Therefore, no additional terms are added.

In this work, the electric potential method is used to compute the Lorentz force $\mathbf{F}_L$. When a magnetic field **B** is applied to the moving conducting material (with electrical conductivity σ), an electric field is generated and the electrical current density **J** can be computed through Ohm's law given as equation (5) below. For a well conducting material the current conservation law is given by equation (6). Therefore, the electric potential Φ satisfies a Poisson equation (equation (7)) from which Φ is calculated. Then, Lorentz force can be computed following equation (8).

$$\mathbf{J} = \sigma\left(-\nabla\Phi + \mathbf{u}\times\mathbf{B}\right) \tag{5}$$

$$\nabla\cdot\mathbf{J} = 0 \tag{6}$$

$$\nabla\cdot\left(\sigma\nabla\Phi\right) = \nabla\cdot\left[\sigma\left(\mathbf{u}\times\mathbf{B}\right)\right] \tag{7}$$

$$\mathbf{F}_L = \mathbf{J}\times\mathbf{B} \tag{8}$$

Note that both the molten steel and the solidified shell are conducting materials and therefore equations (5) to (8) need to be solved in both the liquid steel and shell region. Simply treating the shell as an insulated wall have been seen to lead to unrealistic flow unsteadiness in the mold [5,11]. In this work the above MHD equations are solved in the entire domain that includes the solid shell region.

<u>Computational Methods, Mesh, and Boundary Conditions</u>

The governing equations are solved with an in-house code CUFLOW [9,12–14] which utilizes Graphics Processing Units (GPU). Current version of the code was written using CUDA Fortran, and has been extended to be able to work on multiple GPUs in parallel through the Message Passing Interface (MPI) [14]. In CUFLOW, fractional step method is used to solve the continuity and momentum equations. Pressure and electric potential Poisson equations are solved efficiently by a V-cycle multigrid method, and red-black Successive Over Relaxation (SOR) on GPUs with over-relaxation parameter of 1.6. Details of the solution algorithm are available in reference [9,13,14]. The solver has been validated and used to study the effect of magnetic field in a lid-driven cavity [15] and the flow in the mold region of continuous casters of steel with and without EMBr [5,6]. As listed in Table II, seven simulations were carried out on the Blue Waters supercomputer.

A Cartesian grid of ~16 million finite volume cells (~4 mm cell size) is generated for the computational domain which includes slide gate, SEN and mold region. The domain ends at ~2.8 m below the meniscus. Solid shell is modeled only as an electrically conducting zone (fluid flow equations are not solved) and is included in the domain with a thickness found by the equation $h(\text{mm}) = 3[t(\text{s})]^{1/2}$.

The slide gate was 80% open for a casting speed of 1.8 m/min. The velocity at the SEN inlet is fixed to match the mass flow rate of the steel. At the outlet, a zero derivative boundary condition is applied. All other domain boundaries and the interface between the liquid steel and solidified shell are treated as no slip walls. For the MHD equations, insulated boundary condition was applied at all the boundaries of the computational domain.

Table II. List of the LES simulations

No.	V_c (m/min)	d_{sub} (mm)	Top coil current (A)	Bottom coil current (A)
1	1.8	170	0	0
2	1.8	170	0	850
3	1.8	170	400	850
4	1.8	170	850	850
5	1.8	200	0	0
6	1.8	200	0	850
7	1.8	200	400	850

Validation with Plant Velocity Measurements

In addition to the seven simulations listed in Table II, an 80 second LES simulation with a grid of ~15.5 million cells was conducted for the same casting conditions as the plant measurements. The u_x velocity parallel to WF, at the probe location (1 cm below the top surface and at the quarter mold region in the middle plane) was recorded. Figure 4 compares the measured u_x velocity against the predicted u_x velocity by the LES. Both LES simulation and the SVC-like measurements show that the flow direction was from narrow face (NF) to SEN with an average velocity of ~0.2 m/s. This good agreement between the computational model and the measurements provides support to the code results and demonstrate accuracy of the LES model.

Results and Discussion

Effect of Submergence Depth

Figure 5 shows contours of mean velocity magnitude |**U**| for different submergence depths (d_{sub}) at 1 cm below the top surface and at the center plane of the mold. In the top surface region, the region of high velocity is closer to the Outer Radius (OR) side of the mold. For d_{sub} = 170mm, the maximum velocity is ~0.45m/s. For d_{sub} = 200mm, the maximum top surface velocity is ~0.4m/s and the high velocity region is smaller. Overall, however, flow in the mold is not affected much by submergence depth, as both calculations show double roll flow patterns.

Effect of EMBr

Figure 6 shows the time averaged z-velocity in SEN on the symmetric plane for a submergence depth of 170mm. It is seen that increasing the magnetic field strength in the SEN causes a shorter jet. However, the size of the recirculation region below the sliding gate is not affected much by the magnetic field because the magnetic field strength field in the nozzle is relatively weak (<0.04T). Transient simulations in the mold region show two swirling vortices at the bottom of SEN for all cases except when the upper coil current I_{top} is 850A. The time-averaged flow field also shows two swirling vortices at the bottom of the SEN but only a small swirl for I_{top}=850A.

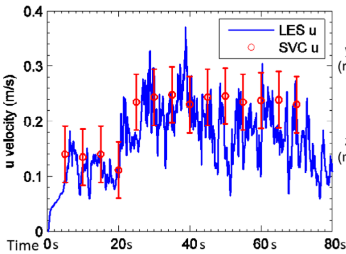

Figure 4. Compare with “SVC”

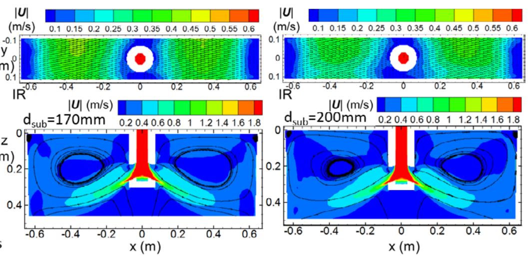

Figure 5. Mean flow in mold and top surface (no EMBr)

Figure 7 shows the time-averaged x-velocity (in/out of port) partway across the port at x = -0.045. A back flow region (where flow enters the port, towards the SEN inside) is seen near the top of port in all cases. With increasing magnetic field, the back flow region becomes larger and occupies almost half of the port when both coils have a current of 850A. The outward flow region is mainly at the bottom half of port, and the speed of the jet in the port increases with increasing magnetic field strength (due to smaller outflow area).

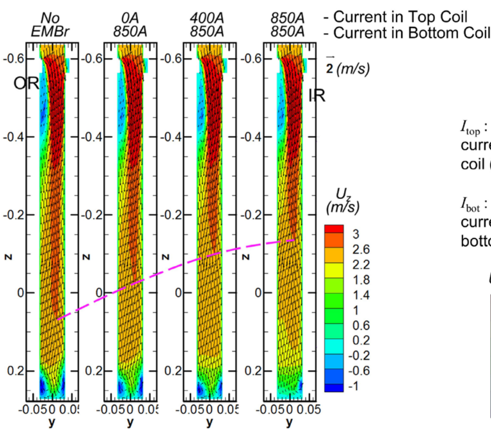

Figure 6. Mean velocity in SEN

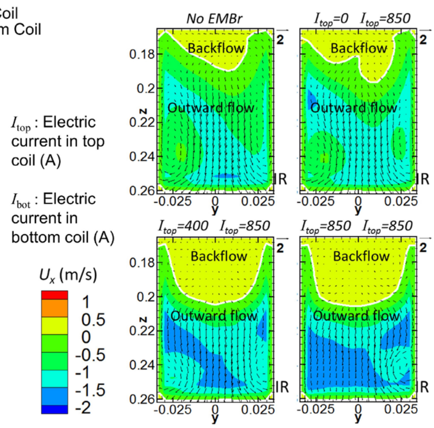

Figure 7. Backflow noticed in port

Contours of the magnitude of the time-averaged velocity in the middle y plane (y=0) for different magnetic fields (d_{sub}=170mm) are shown in Figure 8. With EMBr, thin regions of high velocity appear close to the side walls of the SEN, resulting in an M-shaped velocity profile in the x direction. This M-shaped profile is well known in channel flows with strong magnetic fields [16]. The jets exiting from the port are also thinner and stronger when the EMBr is used. The recirculation regions in the mold are more close to the jet which agrees with previous studies [6].

Figure 9 shows a typical snapshot of contours of velocity magnitude in a horizontal plane z = 0.01m (1cm below top surface). Without EMBr, the maximum velocity is ~0.5m/s and two vortices are seen near the SEN. High velocities and vertical flows at the steel-slag interface may lead to problems such as entrainment of slag. With EMBr (I_{bot}=850A) the top surface velocity drops to ~0.05m/s. This low surface velocity may deliver less superheat to the meniscus region, leading to meniscus solidification, hook formation and entrapment of slag or inclusion particles [17]. Therefore, a weaker magnetic field that maintains the top velocity at around 0.2m/s would be better for this particular caster and casting conditions.

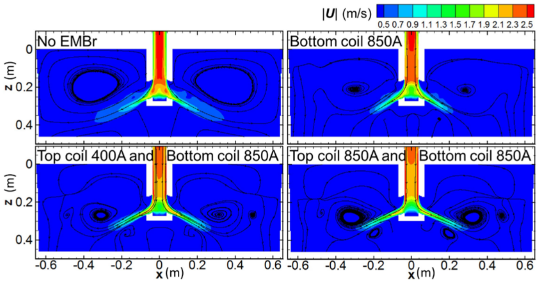

Figure 8. Velocity magnitude in mold and stream traces

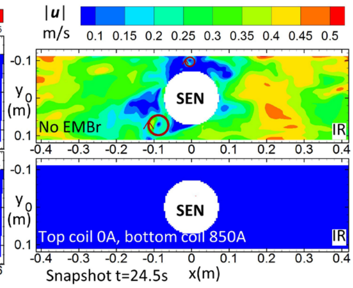

Figure 9. Flow near top surface

Conclusions

LES is used to study the effect of submergence depth and double-ruler EMBr on steel flow in SEN and mold region of a commercial steel caster. The predicted surface velocity history matches well with plant measurements. Applying strong EMBr across the nozzle in this system makes flow inside the SEN more uniform, and increases downward velocity along the walls (with strong EMBr) forming an M-shaped velocity profile in the lower part of the SEN. Application of the EMBr results in a tighter and faster jet in the mold cavity, which exits more towards the lower region of port with accompanying larger back-flow in the top. The recirculation regions in the mold become tighter and closer to the jet and newer smaller vortices form. Even with a high casting speed (1.8m/min) with no argon gas, holding the meniscus level at middle of the top ruler of the EMBr greatly lowers top surface velocity (to ~0.05m/s).

Acknowledgements

The authors thank the financial supports from the National Science Foundation (Grant No. CMMI 11-30882) and the Continuous Casting Consortium, Univ. of Illinois at Urbana-Champaign, USA. Thanks to Baosteel, Shanghai, P.R. China for providing the casting conditions and measurements. This research is also part of the Blue Waters sustained-petascale computing project, which is supported by the National Science Foundation (awards OCI-0725070 and ACI-1238993) and the State of Illinois. Blue Waters is a joint effort of the University of Illinois at Urbana-Champaign and its National Center for Supercomputing Applications. The authors also thank NVIDIA Hardware Grant Program for providing the GPUs for an in-house workstation.

References

1. B. Thomas and R. Chaudhary, “State of the Art in Electromagnetic Flow Control in Continuous Casting of Steel Slabs: Modeling and Plant Validation,” *6th Int. Conf. Electromagn. Process. Mater. EPM* (Dresden, Austria, 2009).

2. A. Idogawa et al., "Control of Molten Steel Flow in Continuous Casting Mold by Two Static Magnetic Fields Imposed on Whole Width," *Mater. Sci. Eng. A*, **173** (1993), 293–297.

3. B. Li, T. Okane, and T. Umeda, "Modeling of Molten Metal Flow in a Continuous Casting Process Considering the Effects of Argon Gas Injection and Static Magnetic-Field Application," *Metall. Mater. Trans. B*, **31** (2000), 1491–1503.

4. Y. Miki and S. Takeuchi, "Internal Defects of Continuous Casting Slabs Caused by Asymmetric Unbalanced Steel Flow in Mold," *ISIJ Int.*, **43** (2003), 1548–1555.

5. R. Chaudhary, B. G. Thomas, and S. P. Vanka, "Effect of Electromagnetic Ruler Braking (EMBr) on Transient Turbulent Flow in Continuous Slab Casting Using Large Eddy Simulations," *Metall. Mater. Trans. B*, **43** (2012), 532–553.

6. R. Singh, B. G. Thomas, and S. P. Vanka, "Large Eddy Simulations of Double-Ruler Electromagnetic Field Effect on Transient Flow during Continuous Casting," *Metall. Mater. Trans. B*, **45** (2014), 1098–1115.

7. S.-M. Cho, S.-H. Kim, and B. G. Thomas, "Transient Fluid Flow during Steady Continuous Casting of Steel Slabs: Part II. Effect of Double-Ruler Electro-Magnetic Braking," *ISIJ Int.*, **54** (2014), 855–864.

8. F. Li et al., "Simulation Research of Flow Field in Continuous Casting Mold with Vertical Electromagnetic Brake," *ISIJ Int.*, **55** (2015), 814–820.

9. R. Chaudhary, "Studies of Turbulent Flows in Continuous Casting of Steel with and without Magnetic Field," PhD Thesis, University of Illinois at Urbana-Champaign, 2011.

10. H. Kobayashi, "Large Eddy Simulation of Magnetohydrodynamic Turbulent Duct Flows," *Phys. Fluids*, **20** (2008), 015102.

11. R. Singh, B. G. Thomas, and S. P. Vanka, "Effects of a Magnetic Field on Turbulent Flow in the Mold Region of a Steel Caster," *Metall. Mater. Trans. B*, **44** (2013), 1201–1221.

12. S. P. Vanka, "2012 Freeman Scholar Lecture: Computational Fluid Dynamics on Graphics Processing Units," *J. Fluids Eng.*, **135** (2013), 061401.

13. A. F. Shinn, "Large Eddy Simulations of Turbulent Flows on Graphics Processing Units: Application to Film-Cooling Flows," PhD Thesis, Univ. of Illinois at Urbana-Champaign, 2011.

14. P. Kumar, K. Jin, and S. P. Vanka, "A Multi-GPU Based Accurate Algorithm for Simulations of Gas-Liquid Flows," *Proc. 1st Therm. Fluids Eng. Summer Conf.* (American Society of Thermal and Fluids Engineers, New York City, August 9).

15. K. Jin, S. P. Vanka, and B. G. Thomas, "Three-Dimensional Flow in a Driven Cavity Subjected to an External Magnetic Field," *J. Fluids Eng.*, **137** (2015), 071104.

16. R. J. Moreau, *Magnetohydrodynamics* (Springer Science & Business Media, 1990).

17. R. Liu et al., "Measurement of Molten Steel Surface Velocity with SVC and Nail Dipping during Continuous Casting Process," *Sens. Sampl. Simul. Process Control* (John Wiley & Sons, San Diego, 2011).